NASA/TM-20220016363

Estimates of Permeability of Water in Rare Earth Silicates Using Modified Theory of Deal and Grove

Roy M. Sullivan, Joshua Stuckner, Kang N. Lee, and Martha H. Jaskowiak
Glenn Research Center, Cleveland, Ohio

January 2023

NASA STI Program . . . in Profile

Since its founding, NASA has been dedicated to the advancement of aeronautics and space science. The NASA Scientific and Technical Information (STI) Program plays a key part in helping NASA maintain this important role.

The NASA STI Program operates under the auspices of the Agency Chief Information Officer. It collects, organizes, provides for archiving, and disseminates NASA's STI. The NASA STI Program provides access to the NASA Technical Report Server—Registered (NTRS Reg) and NASA Technical Report Server—Public (NTRS) thus providing one of the largest collections of aeronautical and space science STI in the world. Results are published in both non-NASA channels and by NASA in the NASA STI Report Series, which includes the following report types:

- TECHNICAL PUBLICATION. Reports of completed research or a major significant phase of research that present the results of NASA programs and include extensive data or theoretical analysis. Includes compilations of significant scientific and technical data and information deemed to be of continuing reference value. NASA counter-part of peer-reviewed formal professional papers, but has less stringent limitations on manuscript length and extent of graphic presentations.

- TECHNICAL MEMORANDUM. Scientific and technical findings that are preliminary or of specialized interest, e.g., "quick-release" reports, working papers, and bibliographies that contain minimal annotation. Does not contain extensive analysis.

- CONTRACTOR REPORT. Scientific and technical findings by NASA-sponsored contractors and grantees.

- CONFERENCE PUBLICATION. Collected papers from scientific and technical conferences, symposia, seminars, or other meetings sponsored or co-sponsored by NASA.

- SPECIAL PUBLICATION. Scientific, technical, or historical information from NASA programs, projects, and missions, often concerned with subjects having substantial public interest.

- TECHNICAL TRANSLATION. English-language translations of foreign scientific and technical material pertinent to NASA's mission.

For more information about the NASA STI program, see the following:

- Access the NASA STI program home page at http://www.sti.nasa.gov

- E-mail your question to help@sti.nasa.gov

- Fax your question to the NASA STI Information Desk at 757-864-6500

- Telephone the NASA STI Information Desk at 757-864-9658

- Write to:
  NASA STI Program
  Mail Stop 148
  NASA Langley Research Center
  Hampton, VA 23681-2199

NASA/TM-20220016363

Estimates of Permeability of Water in Rare Earth Silicates Using Modified Theory of Deal and Grove

Roy M. Sullivan, Joshua Stuckner, Kang N. Lee, and Martha H. Jaskowiak
Glenn Research Center, Cleveland, Ohio

National Aeronautics and
Space Administration

Glenn Research Center
Cleveland, Ohio 44135

January 2023

Acknowledgments

This study was funded by the Hybrid Thermally Efficient Core Project and the Transformational Tools and Technologies Project under NASA's Aeronautics Research Mission Directorate.

This report is a formal draft or working paper, intended to solicit comments and ideas from a technical peer group.

This work was sponsored by the Advanced Air Vehicle Program at the NASA Glenn Research Center

Level of Review: This material has been technically reviewed by technical management.

This report is available in electronic form at https://www.sti.nasa.gov/ and https://ntrs.nasa.gov/

Estimates of Permeability of Water in Rare Earth Silicates Using Modified Theory of Deal and Grove

Roy M. Sullivan, Joshua Stuckner, Kang N. Lee, and Martha H. Jaskowiak
National Aeronautics and Space Administration
Glenn Research Center
Cleveland, Ohio 44135

Summary

The salient elements of the theory of oxide growth under an environmental barrier coating are reviewed. In addition, the results from steam oxidation tests recently conducted on environmental-barrier-coated specimens are reported. The oxide thickness between the ceramic topcoat and silicon bond coat is reported as a function of time. Also, the results from previously conducted steam oxidation tests are reviewed. An approach to estimate the permeability of water vapor through the various coating systems using the oxide thickness versus time measurements and the theory of oxide growth is demonstrated. Although the steam oxidation tests may have been performed under disparate conditions, the approach allows one to rank the protection efficiency of the various coating systems against oxidation of the substrate or silicon bond coat on an equivalent basis.

Introduction

Rare earth silicate coatings are used to protect silicon carbide fiber-reinforced silicon carbide composite (SiC/SiC) components in high-temperature aerospace applications (Lee, Fox, and Bansal, 2005; Lee, 2015; Tejero-Martin, Bennett, and Hussain, 2021). The coatings protect the SiC/SiC components from degradation by active oxidation in environments containing water vapor at high temperatures. A variety of different rare earth silicate coating types have been proposed and investigated. One of the potential threats to the durability of the coating is the diffusion of oxidants such as oxygen or water through the coatings and the formation of a silica layer by passive oxidation of the underlying substrate or bond coat. The coating structural integrity is compromised at some critical silica thickness, so limiting the thickness is essential to extending the life of the coating (Lee, 2019).

Deal and Grove (1965) showed how the rate of oxide thickness growth on uncoated silicon is related to the oxidant permeability of the oxide layer. This relation holds true whether the oxidizing surface is coated or uncoated. Oxidation rates are significantly higher in a steam environment than in a dry air or dry oxygen environment (Deal and Grove, 1965; Lee, 2019), as the permeability of water through silica is higher than the permeability of oxygen (see Norton, 1961, and Moulson and Roberts, 1961). Thus, the current study will focus on oxidation in wet environments.

Recent research studies have performed steam oxidation testing of coated specimens and reported the oxide thickness between the ceramic coating and the oxidizing layer beneath the coating as a function of time (Lee, 2019; Arnal et al., 2022). These studies have investigated various coating formulations. A more recent collaborative study between General Electric Aviation (GE) and the NASA Glenn Research Center performed a similar set of steam oxidation experiments on SiC/SiC composite specimens coated with multiple layers of various rare earth silicates. The results of the previous two steam oxidation studies will be revisited herein, and the results of the latter study will be reported.

Sullivan (2019; 2021) modified the theoretical formulation of Deal and Grove (1965) to account for oxidation of the silicon bond coat under a ceramic coating. It should be noted that these studies are

equally applicable to the oxidation of the substrate in coating systems with no bond coat. Sullivan demonstrated the significant effect of the coating permeability on the rate of oxide growth. Indeed, along with the silica permeability and coating thickness, the coating permeability is one of the three most significant parameters that affect the oxidation rate at a specific temperature and oxidation environment. Measurements of the permeability of oxygen through rare earth silicates have been performed (Wada et al., 2017), but measurements on the permeability of water are rather scarce in the literature. The objective of the current study is to estimate the permeability of water through each of the coating systems using the oxide thickness versus time measurements from the three previously mentioned steam oxidation studies and the equations from Deal and Grove (1965) and Sullivan (2019; 2021).

Review of the Modified Theory of Deal and Grove

The thickness of an oxide scale growing on a free surface can be represented as a function of time with the linear-parabolic equation

$$x_o^2 + Ax_o = B(t + \tau) \tag{1}$$

where x_o is the oxide thickness; t is time; and A, B, and τ are parameters (Deal and Grove, 1965). The τ accounts for the possibility that the oxide thickness may not be zero at time $t = 0$.

The parameter B is known as the parabolic rate constant. Deal and Grove (1965) showed that $B = 2D_{ox}C^*/N_1$, where D_{ox} is the diffusivity of the oxidant through the oxide layer, C^* is the equilibrium concentration of the oxidant in the oxide at the exterior surface, and N_1 is the number of oxidant molecules incorporated into a unit volume of oxide layer. The equilibrium concentration may be represented by Henry's law $C^* = HP$, where H is the solubility and P is the partial pressure of the oxidant in the environment. Using Henry's law and recognizing that the permeability is the product of the solubility and the diffusivity leads to the following expression for the parabolic constant:

$$B = \frac{2\gamma_{ox}P}{N_1} \tag{2}$$

where γ_{ox} represents the permeability of the oxidant in the oxide. The ratio B/A is known as the linear rate constant. Deal and Grove showed that $A \approx 2D_{ox}/k$ where k is the reaction rate constant.

A summary of the values of A, B, and τ reported in Deal and Grove (1965) for oxidation in wet oxygen are listed in Table I. Deal and Grove reported the parameter values as a function of temperature between 920 and 1,200 °C. Both the linear and parabolic rate constants follow an Arrhenius variation with temperature. Plotting the values of $\ln B$ and $\ln B/A$ versus T^{-1} yields the activation energy and pre-exponential coefficient for each rate constant. The values of B and B/A can then be extrapolated to higher temperatures than those reported in Deal and Grove. The values of A and B extrapolated to 1,316 °C are also listed in Table I.

Sullivan (2019) found that, for the growth of an oxide layer under an environmental barrier coating (EBC), the linear-parabolic equation is modified as

$$x_o^2 + \left(A + 2\frac{\gamma_{ox}}{\gamma_c}\delta \right) x_o = B(t + \tau) \tag{3}$$

where γ_c is the oxidant permeability of the coating and δ is the coating thickness. Sullivan (2019) derived

TABLE I.—SUMMARY OF LINEAR-PARABOLIC CONSTANTS REPORTED IN DEAL AND GROVE (1965) FOR OXIDATION IN WET OXYGEN WITH EXTRAPOLATION TO 1,316 °C

Temperature, °C	*A*, μm	*B*, μm²/hr	*B*/*A*, μm/hr	τ, hr
920	0.50	0.203	0.406	0
1,000	0.226	0.287	1.27	0
1,100	0.11	0.510	4.64	0
1,200	0.05	0.72	14.40	0
1,316[a]	0.02536	1.094	43.1308	0

[a]Values at 1,316 °C are extrapolated.

Equation (3) under the assumption that the oxidant transport across the coating was by permeation. Alternatively, Sullivan (2021) examined the problem under the assumption that the oxidant transport across the coating layer was by vacancy diffusion. In the latter approach, an equation with the same form as Equation (3) was obtained, but the coating permeability was replaced by a quantity the author called the effective permeability. Whether the transport is by permeation or vacancy diffusion, both the permeability and the effective permeability of the coating layer can be measured experimentally and calculated using the equation

$$\gamma_c = \frac{J_O}{\Delta P_O / \delta} \tag{4}$$

where J_O is the flux of oxidant through the coating layer and ΔP_O is the oxidant partial pressure differential across the coating layer.

The terms in brackets in Equation (3) were denoted as A' in Sullivan (2019). For EBC systems with more than one topcoat layer, this can be written as

$$A' = A + 2\gamma_{ox} \sum_{i=1}^{N} \frac{\delta_i}{\gamma_{c,i}} \tag{5}$$

where N is the number of coating layers and δ_i and $\gamma_{c,i}$ are the thickness and permeability of the i^{th} layer, respectively. One may define a weighted average permeability of the layered system as

$$\overline{\gamma}_c = \frac{\delta_{tot}}{\sum_{i=1}^{N} \frac{\delta_i}{\gamma_{c,i}}} \tag{6}$$

where δ_{tot} is the sum of the coating layer thicknesses. Equation (5) may therefore be rewritten as

$$A' = A + 2\frac{\gamma_{ox}}{\overline{\gamma}_c}\delta_{tot} \tag{7}$$

Oxide Growth Experimental Data

Lee (2019) coated SiC/SiC composite specimens with a two-layered system consisting of a silicon bond coat and a ytterbium disilicate (YbDS, $Yb_2Si_2O_7$) topcoat. Lee investigated the effect of various additives to the topcoat on the rate of silica growth between the topcoat and the bond coat. The bond coat had a nominal thickness of 125 μm, and the topcoat layer had a thickness of 254 μm. The specimens were placed in an environment of 90 percent H_2O and 10 percent O_2 and thermally cycled. Each thermal cycle consisted of a 1-hr hold at 1,316 °C and then a 20-min cooling period to temperatures less than 200 °C. Lee compared the oxide growth of the various formulations to the growth under the baseline $Yb_2Si_2O_7$ formulation (Glenn Gen 2 Baseline YbDS). Some of the $Yb_2Si_2O_7$ formulations resulted in a decrease in the oxide growth rate compared to the baseline YbDS formulation, and some of the formulations resulted in an increase in the growth rate compared to the baseline. The measured oxide thickness versus time for the Glenn Gen 2 Baseline YbDS formulation and two of the modified topcoat formulations (referred to as "Glenn Gen 2 YbDS AT" and "Glenn Gen 2 YbDS M") reported in Lee are plotted as the individual data points in Figure 1.

Arnal et al. (2022) coated silicon pellets with yttrium monosilicate and yttrium disilicate coatings and exposed the coated pellets to an oxidizing environment of 10 kPa O_2, 50 kPa H_2O, and 40 kPa N_2 and a temperature of 1,300 °C. Specifically, the coatings were (1) yttrium disilicate with a grain size of 0.8 μm (Univ. of Bordeaux YDS 0.8 μm), (2) yttrium disilicate with a grain size of 3 μm (Univ. of Bordeaux YDS 3 μm), and (3) yttrium monosilicate with a grain size of 0.8 μm (Univ. of Bordeaux YMS 0.8 μm). The coating thickness for all specimens was approximately 500 μm. They measured the thickness of the oxide that grew on the silicon substrate and underneath the yttrium coatings as a function of time. The measured oxide thickness for the three coating types reported by Arnal et al. is plotted versus

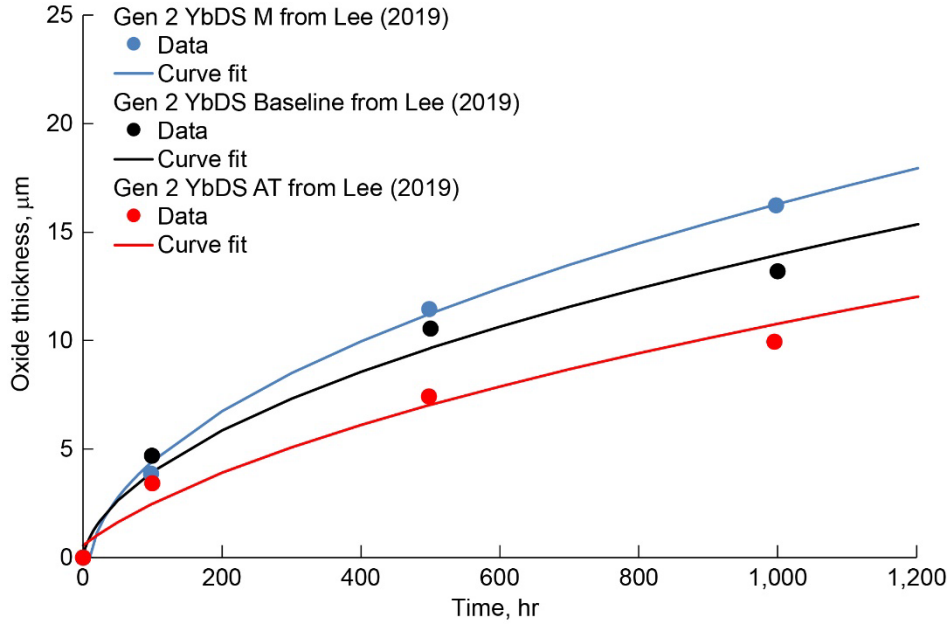

Figure 1.—Oxide thickness versus time for specimens with ytterbium disilicate coatings on silicon bond coat: Gen 2 YbDS Baseline and two modified, Gen 2 YbDS AT and Gen 2 YbDS M, in environment of 90 percent H_2O and 10 percent O_2 and thermal cycling of 1,316 °C for 1 hr then 20 min cooling to temperatures less than 200 °C. Data points are measurements reported in Lee (2019). Solid lines are plots of Equation (3), using optimized values for A', B, and τ.

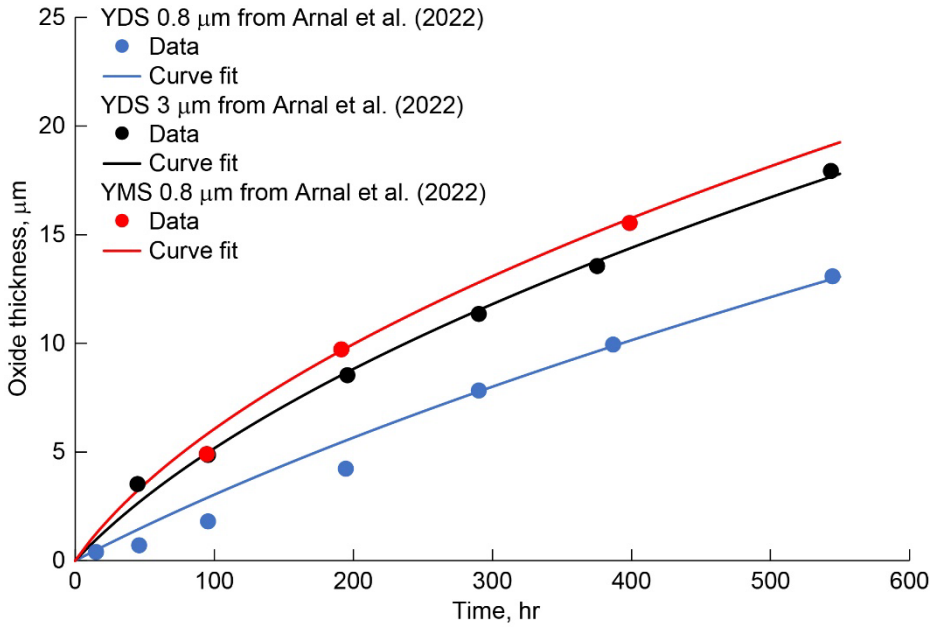

Figure 2.—Oxide thickness versus time at constant temperature for specimens with yttrium disilicate coatings: YDS 0.8 μm and YDS 3 μm, and yttrium monosilicate coating YMS 0.8 μm, on silicon at 1,300 °C in environment of 10 kPa O_2, 50 kPa H_2O, and 40 kPa N_2. Data points are measurements reported in Arnal et al. (2022). Solid lines are plots of Equation (3), using optimized values for A', B, and τ.

time as the individual data points in Figure 2. The coating that provided the best protection from oxide scale growth was the yttrium disilicate coating with a 0.8-μm grain size, and the coating with the least effective protection was the yttrium monosilicate coating.

Steam oxidation experiments were recently performed on EBC-coated SiC/SiC composite specimens in a collaborative study by GE and NASA Glenn. The specimens were coated by GE, and the steam oxidation testing was performed by Glenn. The specimens were placed in an environment of 90 percent H_2O and 10 percent O_2 and thermally cycled. Each thermal cycle consisted of a 1-hr hold at 1,316 °C and then a 20-min cooling period to temperatures less than 200 °C. Three EBC systems were investigated: the baseline coating system (GE Baseline), the Architecture 1 system (GE Arch 1), and the Architecture 2 system (GE Arch 2). All EBC systems used a silicon bond coat with a nominal thickness of 100 μm. The GE Baseline coating system was a double-layered system consisting of a rare earth disilicate layer and a rare earth monosilicate layer, with a total thickness of 356 μm. The GE Arch 1 system was also a double-layered system, consisting of two different rare earth disilicate layers with a total thickness of 356 μm. The GE Arch 2 system was a single rare earth disilicate coating with a thickness of 305 μm. The chemistries of the rare earth disilicate and monosilicate systems are proprietary and thus not reported here. The thickness of the silica layer that grew on the silicon bond coat for all three EBC systems was measured at 500, 1,000, and 2,000 hr. The average silica layer thickness for the three EBC systems are plotted versus time as the individual data points in Figure 3.

The data points for each of the coating systems in Figure 1 to Figure 3 were fit to the linear-parabolic growth equation (Eq. (3)), and a residual sum-of-squares minimization was performed to obtain the optimized values for the parameters B, A', and τ. The optimized values of B, A', and τ for each of the coating systems are listed in Table II. The linear-parabolic equation using the optimized values for the three parameters is plotted for each coating as the solid lines in Figure 1 to Figure 3. The optimization for

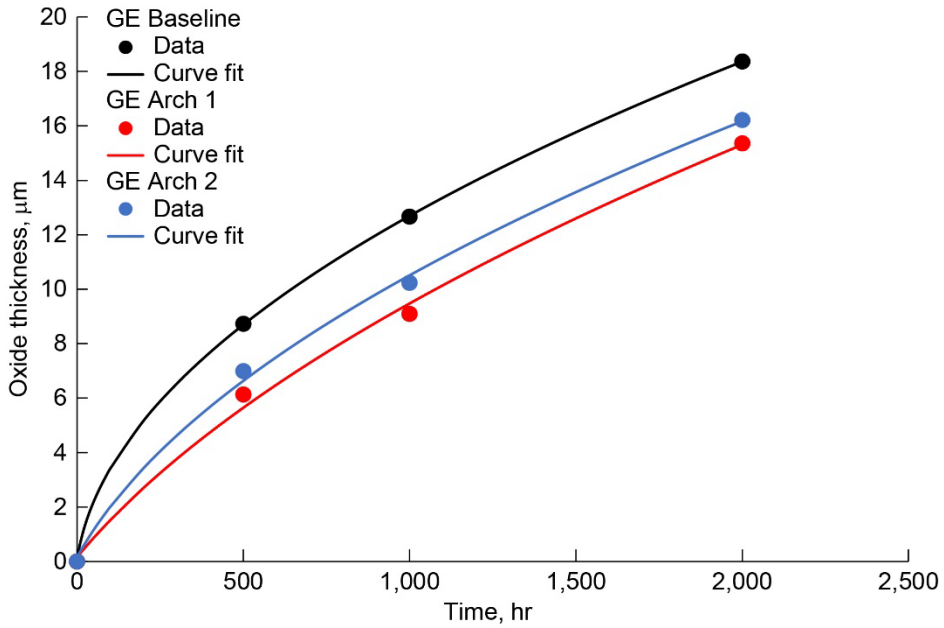

Figure 3.—Oxide thickness versus time for specimens with rare earth silicate coatings on silicon bond coat: GE Baseline, GE Arch 1, and GE Arch 2 environmental barrier coatings, in environment of 90 percent H_2O and 10 percent O_2 and thermal cycling of 1,316 °C for 1 hr then 20 min cooling to temperatures less than 200 °C. Data points are measurements reported in current study. Solid lines are plots of Equation (3), using optimized values for A', B, and τ.

all coating systems was performed with no constraints on the parameters, except for two of the formulations reported in Lee (2019). The initial optimizations for the Gen 2 Baseline YbDS and the modified YbDS AT formulations from Lee each produced a negative value for the parameter A', which, of course, is not physically realistic. The optimization for the baseline and the AT modified formulations were repeated with certain constraints placed on the parameters in order to obtain positive values for A'. The baseline optimization was performed with the constraint $A' \geq 1.6$, and the AT modification optimization was performed with the constraint $B \geq 0.18$.

Permeability Calculations

From the values of A' in Table II and the value of A at 1,316 °C in Table I, it appears that $A' \gg A$ for all the coating systems listed in Table II. Therefore, one may make the approximation that $A' \approx 2(\gamma_{ox}/\gamma_c)\delta$ for the test specimens with one coating layer and $A' \approx 2(\gamma_{ox}/\overline{\gamma}_c)\delta_{tot}$ for the specimens with multiple layers. These approximations were used to obtain the permeability ratios γ_c/γ_{ox} or $\overline{\gamma}_c/\gamma_{ox}$ for all of the cases listed in Table II. The permeability ratios are listed as the third-to-last and second-to-last columns in Table II. The permeability ratios indicate that the permeability of water is higher in the coating than in the silica layer for all coating systems. In some cases, the permeability of water in the coating is more than 300 times greater than in the silica layer.

TABLE II.—ASSESSMENT OF RESULTS FROM THREE EXPERIMENTAL STUDIES MEASURING OXIDATION OF SILICON IN ENVIRONMENTAL BARRIER COATING SYSTEMS WITH ESTIMATES OF COATING PERMEABILITY

Source	Environment	Temperature, °C	Oxidizing substrate	Coating	Pressure, P, atm	Coating thickness, δ or δ_{tot}, μm	Parameters			Permeability ratios		Coating permeability, γ_c or $\overline{\gamma}_c$, mole/(cm-atm-sec)
							B, $\mu m^2/hr$	A', μm	τ, hr	γ_c/γ_{ox}	$\overline{\gamma}_c/\gamma_{ox}$	
Lee (2019)	90% H_2O 10% O_2	1,316	Si bond coat	Glenn Gen 2 YbDS Baseline[a]	0.9	254	0.2167	1.6	1.245	317.5	-------	7.94×10^{-12}
				Glenn Gen 2 YbDS AT[b]	0.9	254	0.18	6.296	21.166	80.686	-------	1.68×10^{-12}
				Glenn Gen 2 YbDS M	0.9	254	0.2928	1.5058	–9.803	337.36	-------	1.14×10^{-11}
Arnal et al. (2022)	10 kPa O_2 50 kPa H_2O 40 kPa N_2	1,300	Si pellet	Univ. of Bordeaux YDS 0.8 μm	0.5	500	1.13	33.879	–1.489	29.517	-------	6.93×10^{-12}
				Univ. of Bordeaux YDS 3 μm	0.5	500	1.31	22.811	8.939	43.838	-------	1.19×10^{-11}
				Univ. of Bordeaux YMS 0.8 μm	0.5	500	1.18	14.382	–3.72	69.53	-------	1.70×10^{-11}
Current study	90% H_2O 10% O_2	1,316	Si bond coat	GE Baseline	0.9	356[c]	0.1879	2.118	0.623	-------	336.166	7.29×10^{-12}
				GE Arch 1	0.9	356[c]	0.2362	15.723	10.991	-------	45.284	1.23×10^{-12}
				GE Arch 2	0.9	305	0.1998	8.632	7.061	70.667	-------	1.63×10^{-12}

[a]Optimization performed with constraint $A' \geq 1.6$.
[b]Optimization performed with constraint $B \geq 0.18$.
[c]Total of multiple coating thicknesses.

Table II also reveals a distinct difference in the value of B between the experiments that oxidized a silicon bond coat (Lee (2019) and the NASA–GE collaboration) and the experiments that oxidized silicon pellets (Arnal et al., 2022). Recall from Equation (2) that parameter B is a function of the partial pressure of the oxidant in the environment and the permeability of the oxidant in the oxide. The fact that the different test series produced different values for B is not surprising, since the oxidation of different types of silicon can produce different forms of silica, which may then possess different values of permeability. There is also a difference in the partial pressure of the oxidant in the environment between the Arnal et al. tests and the other two test series. Note that the value of the parabolic rate constant obtained from the Arnal et al. tests is similar to that obtained from extrapolation to 1,316 °C in Table I. The parabolic rate constants reported in Deal and Grove were obtained from oxidation tests conducted on single-crystal silicon wafers.

In order to estimate the permeability of the coating systems in Table II, the permeability ratios were multiplied by the permeability of the oxide for each test case. Rewriting Equation (2) as $\gamma_{ox} = BN_1/2P$, the coating permeability is calculated as

$$\gamma_c = \frac{\gamma_c}{\gamma_{ox}} \frac{BN_1}{2P} \tag{8a}$$

for single-coated specimens and

$$\overline{\gamma}_c = \frac{\overline{\gamma}_c}{\gamma_{ox}} \frac{BN_1}{2P} \tag{8b}$$

for specimens with multiple coats. For the oxidation of silicon by water $N_1 = 4.5\times10^{22}$ cm^{-3}. The estimated permeability of all coating systems is listed as the last column in Table II. The coating systems are ranked in order of lowest to highest permeability in Table III.

TABLE III.—RANKING OF COATING SYSTEMS FROM LOWEST TO HIGHEST PERMEABILITY

Coating system	Permeability, mole/(cm-atm-sec)
GE Arch 1	1.23×10^{-12}
GE Arch 2	1.63×10^{-12}
Glenn Gen 2 YbDS AT	1.68×10^{-12}
Univ. of Bordeaux YDS 0.8 μm	6.93×10^{-12}
GE Baseline	7.29×10^{-12}
Glenn Gen 2 Baseline YbDS	7.94×10^{-12}
Glenn Gen 2 YbDS M	1.14×10^{-11}
Univ. of Bordeaux YDS 3 μm	1.19×10^{-11}
Univ. of Bordeaux YMS 0.8 μm	1.70×10^{-11}

Concluding Remarks

The preceding discussion has demonstrated how the equations that result from the modified theory of Deal and Grove can be used to estimate the permeability of coatings and coating systems from the oxide thickness versus time measurements. This provides a metric to rank the protection efficiency of various coating systems regardless of whether the steam oxidation tests are conducted at different environmental partial pressures, involve different oxidizing substrates, or have different coating thicknesses. It was determined that for all coating systems, the permeability of water in the coatings is higher than the permeability of water in the silica layer.

References

Arnal, S., et al. (2022): Design of a New Yttrium Silicate Environmental Barrier Coating (EBC) Based on the Relationship Between Microstructure, Transport Properties and Protection Efficiency. J. Eur. Ceram., vol. 42, no. 3, pp. 1061–1076.

Deal, B.E.; and Grove A.S. (1965): General Relationship for the Thermal Oxidation of Silicon. J. Appl. Phys., vol. 36, no. 12, pp. 3770–3778.

Lee, Kang N.; Fox, Dennis S.; and Bansal, Narottam P. (2005): Rare Earth Silicate Environmental Barrier Coatings for SiC/SiC Composites and Si_3N_4 Ceramics. J. Euro. Ceram. Soc., vol. 25, no. 10, pp. 1705–1715.

Lee, Kang N. (2015): Special Issue: Environmental Barrier Coatings. Coatings, vol. 10, no. 6, article no. 512.

Lee, Kang N. (2019): $Yb_2Si_2O_7$ Environmental Barrier Coatings With Reduced Bond Coat Oxidation Rates via Chemical Modifications for Long Life. J. Am. Ceram. Soc., vol. 102, no. 3, pp. 1507–1521.

Moulson, A.J.; and Roberts, J.P. (1961): Water in Silica Glass. Trans. Faraday Soc., vol. 57, pp. 1208–1216.

Norton, Francis J. (1961): Permeation of Gaseous Oxygen Through Vitreous Silica. Nature, no. 4789, p. 701.

Sullivan, Roy M. (2019): Reformulation of Oxide Growth Equations for Oxidation of Silicon Bond Coat in Environmental Barrier Coating Systems. J. Eur. Ceram., vol. 39, no. 16, pp. 5403–5409.

Sullivan, R.M. (2021): On the Oxidation of the Silicon Bond Coat in Environmental Barrier Coatings. J. Eur. Ceram., vol. 41, pp. 557–562.

Tejero-Martin, Daniel; Bennett, Chris; and Hussain, Tanvir (2021): Review on Environmental Barrier Coatings: History, Current State of the Art and Future Developments. J. Eur. Ceram. Soc., vol. 41, pp. 1747–1768.

Wada, Masashi, et al. (2017): Mass Transfer in Polycrystalline Ytterbium Disilicate Under Oxygen Potential Gradients at High Temperatures. Acta Mater., vol. 135, pp. 372–381.